Theoretical Study of Two-State Reactivity of Transition Metal Cations: The "Difficult" Case of Iron Ion Interacting with Water, Ammonia, and Methane

Sandro Chiodo, Olga Kondakova, Maria del Carmen Michelini, Nino Russo,* and Emilia Sicilia

Dipartimento di Chimica and Centro di Calcolo ad Alte Prestazioni per Elaborazioni Parallele e Distribuite-Centro d'Eccellenza MURST, Università della Calabria, I-87030 Arcavacata di Rende, Italy

Arantxa Irigoras

Humanitate eta Hezkuntza Zientzien Fakultatea, Mondragon Unibertsitatea, Dorleta auzoa, 20540 Eskoriatza, Euskadi, Spain

Jesus M. Ugalde

Kimika Fakultatea, Euskal Herriko Unibertsitatea, P.K. 1072, 20080 Donostia, Euskadi, Spain

Received: August 28, 2003; In Final Form: December 4, 2003

The potential energy surfaces corresponding to the dehydrogenation reaction of H_2O, NH_3, and CH_4 molecules by $Fe^+(^6D, ^4F)$ cation have been investigated in the framework of the density functional theory in its B3LYP formulation and employing a new optimized basis set for iron. In all cases, the low-spin ion−dipole complex, which is the most stable species on the respective potential energy hypersurfaces, is initially formed. In the second step, a hydrogen shift process leads to the formation of the insertion products, which are more stable in a low-spin state. From these intermediates, three dissociation channels have been considered. All of the results have been compared with existing experimental and theoretical data. Results show that the three insertion pathways are significantly different, although spin crossings between high- and low-spin surfaces are observed in all cases. The topological analysis of the electron localization function has been used to characterize the nature of the bonds for all of the minima and transition states along the paths.

I. Introduction

Reactions of first-row transition metal single-charged cations with compounds containing prototypical bonds (e.g., C−H, C−C, N−H, O−H) have been the focus of a great deal of attention in the past years.[1−26] This interest is mainly attributable to the role that bond activation reactions play in various areas of chemical research as organic chemistry, biochemistry, and, most importantly, catalytic processes. The gas-phase is the ideal environment to study this kind of reaction, both experimentally and theoretically, under controlled conditions and without disturbing factors such as the presence of the solvent, strong intermolecular interactions, and crystal forces. From an experimental point of view, a wealth of exhaustive information, particularly derived from mass-spectrometric measurements, has been accumulated in the course of the years.[1−26] However, despite the enormous amount of experimental data regarding this subject, an accurate description of the reaction mechanism, i.e., in terms of elementary steps, structural and energetical characterization of intermediates and transition states, cannot be achieved by using experimental determinations only. Accurate theoretical computations can offer an alternative source of information and, as it has been plentifully demonstrated,[27−35] the strong interplay between theory and experiment is very helpful in this area of research.

Another topic of interest in reactions that involve first-row transition metal cations is the presence of many low-lying excited states and then, the involvement in their peculiar reactivity of at least two spin states of which the ground state is not necessarily the most reactive one. To classify these reactions, which involve participation of more than a single spin surface, the two-state reactivity (TSR) paradigm has been introduced recently.[36] More than one spin surface is admitted to connect reactants and products, and spin crossover along the reaction coordinate occurs. The idea of state-selective reactivity was introduced, at first, by Armentrout and co-workers,[37,38] who have also pointed out the possible effects that may determine this behavior. Electronic energy content, spin conservation, and electron configuration, at least, could be invoked to rationalize the reactivity of bare metal ions with neutrals.

Extensive experimental and theoretical works have been carried out regarding the reactivity of iron cation with small molecules, and here we mention only the most relevant for our purposes. The gas-phase chemistry of transition metal ions with ammonia was explored by Bruckner et al.[39] using a Fourier transform ion cyclotron. The reaction of first transition series metal ions, Sc^+ through Zn^+, with small saturated hydrocarbons such as methane was studied in a multicollisional environment.[40] Guided ion beam mass spectrometry was used by Armentrout et al. to study the activation of methane by iron[41] in different electronic states. The same reaction, and its reverse $FeCH_2^+ +$

* To whom correspondence should be addressed. E-mail: nrusso@unical.it.

10.1021/jp036558l CCC: $27.50
Published on Web 01/17/2004

H_2, was reexamined by Haynes et al.[42] The results for the reverse process were compared with those obtained previously by Jacobson and Freiser.[43] Finally, bond dissociation energies (BDEs) of M^+-NH_3 complexes of first-row transition metals, including iron, have been determined by examining their collision-induced dissociation reactions.[44]

On the theoretical side, CASSCF and MR−SDCI−CASSCF methods in conjunction with a very limited quality basis set were used to study[45] the molecular and electronic structures of $FeCH_2^+$, as well as the mechanism of the reaction of Fe^+ with CH_4. The same CASSCF method combined with gradient techniques has been used to study the stability of the low-spin hydridomethyl complexes, $HMCH_3^+$, of the first-row transition metal cations.[46] Geometries, electronic structures, and binding energies of these species, which are regarded as stable intermediate in the insertion reactions into the C−H bond, have been reported together with those of the transition states leading to them. Several quantum mechanical tools have been used to study in detail the binding of the iron cation with methane. For example, Bauschlicher et al. have used both DFT and numerous post-HF approaches to deeply investigate the properties of the $FeCH_4^+$ complex.[47,48] The properties of the adducts formed upon interaction of ammonia with the monopositive d-block metal ions of interest have been calculated by using a modified extended Huckel molecular orbital model,[49] and their binding energies were also determined using the modified coupled-pair functional approach.[50]

The presence in the literature of the exhaustive studies, carried out by the Donostia group, on the mechanism of the water dehydrogenation reactions by first-row transition metal ions,[28−31] iron included, gives us the opportunity to compare the similarities and differences in reactivity of the same metal center toward different small ligands. Indeed, water, ammonia, and methane represent a good correlated group of molecules, whose central atom possesses the same sp^3 hybridization and number of valence electrons but a different number of lone pairs, two on oxygen, one on nitrogen, and none on carbon. The former factor can be considered responsible for the similarities observed in the behaviors along the paths, whereas differences, particularly in the energetics, can be ascribed to the latter one.

Previous works performed by the Calabria group[33−35] agreed with experimental findings concerning the reactivity of the early (Sc^+, Ti^+, and V^+) and middle (Cr^+, Mn^+) transition metal cations with ammonia and methane, and here we extend our investigation to include iron cation also and the comparison of its reactivity with water, with the aim to contribute to a better understanding of observed periodic trends and reactivity patterns.

Experimentally, it has been shown that three main reactions are observed to occur when transition metals ions interact with water, ammonia, and methane, with branching ratios varying across the periodic table:

$$M^+ + XH_n \longrightarrow \begin{cases} MXH_{n-2}^+ + H_2 & (1) \\ MH^+ + XH_{n-1} & X=C,N \quad (2) \\ MXH_{n-1}^+ + H & (3) \end{cases}$$

The H_2 elimination process is the most thermodynamically favored, for early and middle metals, whereas at higher energies, the other reaction products became accessible. The mechanism proposed on the basis of experimental analysis involves formation of an ion−dipole complex with no activation energy barrier followed by activation of one H−X (X = N, C) bonds leading to the insertion complex, whose formation is the key step of the overall process. To analyze the proposed mechanism, in this work, the electronic and molecular structures of the various compounds implicated in the insertion reactions of Fe^+ into O−H, N−H, and C−H bonds of water, ammonia, and methane, have been determined by using density functional theory (DFT). The calculated reaction paths have been compared with the PES for water activation explored at the CCSD(T) level of theory.[29] Contemporary, a newly developed DZVP basis set for iron has been employed to recalculate DFT reaction pathways for water, ammonia, and methane activation. This kind of basis set, developed for all of the 3d elements of the series solves the well-known problems, attributed to a bias toward $3d^n$ over $3d^{n-1}4s^1$ configurations,[51] met by DFT in the description of atomic ground states.

II. Method

Geometry optimizations as well as frequency calculations for all of the stationary points considered here have been performed at the density functional level of theory, employing the hybrid B3LYP[52,53] functional, together with the DZVP[54a] (for the transition metals) and TZVP[54b] (for the other atoms) sets. For each optimized stationary point, vibrational analysis was performed to determine its character (minimum or saddle point) and to evaluate the zero-point vibrational energy (ZPVE) corrections, which are included in all relative energies. For transition states, it was carefully checked that the vibrational mode associated to the imaginary frequency corresponds to the correct movement of involved atoms. In addition, paths connecting transition states to the minima were explored by using the intrinsic reaction coordinate (IRC)[55] path following tool.

Previous investigations on transition metal compounds have indicated, without any doubt, that the performance of the B3LYP DF in predicting numerous properties such as binding energies, geometries, frequencies, and the like is very satisfactory. Moreover, although the accuracy of the results is comparable to that obtainable by highly correlated ab initio methods, substantially less demanding computational efforts are required.[56−62] However, the problems inherent in density functionals are particularly evident in the case of iron, for which an incorrect ordering of the ground, ^6D (sd^6), and the excited, ^4F (d^7), states is predicted. Several correction schemes[59] have been proposed to take into account the experimental value of the splitting and the d orbitals populations, but the same schemes seem to not work properly[63] when applied to other cations of the series. For this reason, with the purpose to give a reliable description of the quantitative features of the PESs, a completely new developed basis set for iron atom, optimized for the B3LYP functional, has been employed to localize minima and transition states relevant for the examined processes and to investigate the corresponding potential energy surfaces. This basis set has been built-up starting from the corresponding DZVP one,[54a] obtained within the local density approximation, optimizing variationally[64] the linear combination coefficients, which define a contracted function, and will be described briefly as follows. The initial basis set of the atom is assumed to have the expansion pattern (k_{s1},k_{s2}...k_{sn}/k_{p1},..k_{pn}/k_{d1}..k_{dn}), where k_{li} denotes the number of GTOs in the ith contraction (CGTO) of l symmetry. The CGTO can be expressed as: $l_i = \sum_{j=1}^{k_{li}} d_{li,j} g_{li}(\alpha_{li}, j; r)$, where g_{il} denotes a GTO. In the first step of the procedure, all s, p, and d type CGTOs are decontracted, except the s_1, and the coefficients d_{li} are optimized through SCF procedure adopting the chosen specific functional, that in the examined case was the B3LYP one. The new set of coefficients is substituted to the old one and the s_2 is contracted. The procedure is repeated for all of the contraction coefficients of the CGTOs leaving the decontraction of s_1 and the optimization of its coefficients as

TABLE 1: Exponents and Contraction Coefficients Relative to the B3LYP Optimized DZVP Basis Set

subset	exponents	contraction coefficients
s	61430.2300000000	0.001750
	9222.1760000000	0.013400
	2097.5970000000	0.066600
	591.4904000000	0.227930
	191.8606000000	0.468450
	65.8263200000	0.359940
s	128.7407000000	−0.109450
	14.7181300000	0.646650
	5.9507540000	0.458490
s	10.8598800000	−0.247080
	1.7194470000	0.761770
	0.6664531000	0.381200
s	0.9754761000	−0.166830
	0.1231143000	0.720910
s	0.0448795000	1.000000
p	780.6203000000	0.009090
	184.0062000000	0.067500
	58.0844700000	0.257660
	20.7597900000	0.504650
	7.5934510000	0.339240
p	4.0279170000	0.350950
	1.5264700000	0.611540
	0.5573702000	0.240890
p	0.1210000000	1.000000
d	23.9293200000	0.054690
	6.3999010000	0.239370
	1.9317420000	0.437070
	0.5115279000	0.386470
d	0.0900000000	1.000000

the last step of the procedure that can be repeated until the total energy stabilizes within a certain threshold. In comparison to the traditional DZVP basis set, the new one, whose exponents and contraction coefficients are given in Table 1, improves the description of the ground and low lying excited energy levels of iron cation. We will refer to this level of computation as B3LYP/DZVP$_{opt}$.

The counterpoise corrections[65] have been calculated at the B3LYP/DZVP$_{opt}$ level for all of the ion−dipole complexes formed at the entrance channel to correct binding energies (BE) for basis set superposition error (BSSE). The introduced corrections appear to be negligible and, in all cases, less than one kcal/mol. This result reinforces the belief that the used basis set is good enough to be used for this kind of calculations.

All the calculations reported in the present work have been carried out with the Gaussian 94/DFTcode.[66]

A topological description of all of the key minima and transition states that we have found along the potential energy surfaces has been made in order to characterize the bonding. In particular, we have used the topological analysis of the chemical bond proposed by Silvi and Savin,[67] which relies upon the gradient field analysis of the electron localization function (ELF) of Becke and Edgecombe.[68] The applications of this method to the understanding of the chemical bond[69,70] and reactivity in terms of elementary catastrophes[71−73] are well documented.

The analysis of the ELF gradient field provides a mathematical model enabling the partition of the molecular position space in basins of attractors, which present in principle a one to one correspondence with chemical local objects such as bonds and lone pairs. These basins are either core basins, labeled C(A), or valence basins, V(A,...), belonging to the outermost shell and characterized by their coordination number with core basins, which is called the synaptic order. In a recent work,[74] we have found that this method is a reliable tool to analyze the nature of the chemical bonds present in the systems of interest. ELF calculations have been carried out with the TopMod package developed at the Laboratoire de Chimie Théorique de l'Université Pierre et Marie Curie.[75,76] Isosurfaces have been visualized with the public domain scientific visualization and animation program for high performance graphic workstations named SciAn.[77]

TABLE 2: Relative Energies, in kcal/mol, for the ^{4}F (d^7) Excited State of Fe$^+$ Cation with Respect to the ^{6}D (sd^6) Ground State

method	gap
B3LYP/DZVP[a]	−10.47
B3LYP/TZVP+G(3df,2p)[a]	−4.22
B3LYP/ DZVP$_{opt}$	12.40
CCSD(T)[a]	5.39
exp.[b]	5.77

[a] Reference 29. [b] Reference 78.

III. Results and Discussion

A. Excitation Energy. The experimental[78] ground state of the iron cation is ^{6}D, derived from a 4s3d^6 electronic configuration, lower only 5.76 kcal/mol than the ^{4}F (3d^7) first excited state.

In Table 2, the excitation energy of the iron cation predicted by various levels of theory is given. The incorrect prediction, at the B3LYP level, of the ordering of the states for Fe$^+$ illustrates one of the major shortcomings, extensively discussed in the literature,[48,58,79,80] of the DFT approach no matter whether pure or hybrid. The stability order of the first excited state with respect to the ground state is correctly provided by the CCSD(T) method,[29] which also reasonably reproduces the value of the experimental gap. As Table 2 shows, with the basis set optimized for the hybrid B3LYP functional, the correct ground state of the iron cation is predicted, even if the value of the gap is overestimated. This result encouraged us to check the performance of the new iron B3LYP-optimized basis set in predicting structural, electronic, and energetic properties of the complexes along the Fe$^+$ activation paths. The iron ^{6}D asymptote has been used as the reference state for energy calculations at all of the levels of theory, including the B3LYP/DZVP one.

B. Calibration. With the purpose to asses the accuracy of the employed computational strategies, we have compared experimental and theoretical metal−ligand bond strengths of the reaction fragments of the various exit channels for the interaction of the Fe$^+$ cation with water, ammonia, and methane. Table 3 summarizes the experimentally determined[23,24,41,81−84] and the theoretically predicted bond dissociation energies (BDE). At a first glance, it appears that BDEs provided by using the B3LYP functional do not fit the experimental values for the traditional DZVP basis set, optimized for the local-only functional. As the binding energies are calculated with respect the ^{6}D ground-state asymptote of Fe$^+$, any error present in the calculation of the excitation energy is likely to remain in the binding energies. A significant improvement is obtained with the newly developed basis set.

C. Potential Energy Surfaces. The mechanism, most consistent with experimental observations, of the reactions of metal ions, M$^+$, with water, ammonia, and methane (XH$_n$ (X = O, N, C)) involves formation in the first step of a stable ion−dipole complex. In this adduct, one H−X bond is activated and an insertion is realized through a transition state corresponding to a hydrogen shift from the X atom to the metal center. The H−Fe$^+$−XH$_{n-1}$ insertion intermediate plays a key role in the whole process. Indeed, due to the presence of two covalent H−Fe and Fe−N bonds, two of the valence electrons of the metal are involved in bonding, leading to a low-spin ground

TABLE 3: Metal−Ligand Bond Dissociation Energies for the Reaction Products of the Various Exit Channels with Respect to the Sextet Ground State[a]

level of theory	FeO^+	$FeOH^+$	$FeNH_2^+$	$FeCH_2^+$	$FeCH_3^+$	FeH^+
B3LYP/DZVP	66.9	90.4	72.5	90.7	68.1	63.7
B3LYP/$DZVP_{opt}$	72.7	80.2	74.4	78.2	57.9	52.1
exp.	80.0 ± 1.4[b]	87.4 ± 2.8[c]	73.8 ± 2.3[d]	81.6 ± 1.8[e]	54.6 ± 1.1[f]	48.9 ± 1.4[g]

[a] All of the values are in kcal/mol. [b] Reference 81. [c] Reference 23. [d] Reference 24. [e] Reference 82. [f] References 41 and 83. [g] Reference 84.

state for this species. If the ground state of the cation is a high one, the spin is not conserved along the path and a surface crossing is likely to occur. After this step, the reaction, can proceed toward the formation of dehydrogenation products, through a concerted four-center elimination of H_2 corresponding to a second transition state, or the formation of MH^+ and MXH_{n-1} species, as the result of simple cleavage of M−X and M−H bonds in the insertion intermediate.

An alternative proposed mechanism involves the formation of the insertion intermediate followed by α-H migration to M^+ to form the covalently bonded intermediate, $(H)_2-M^+-XH_{n-2}$, and reductive elimination of H_2. On the basis of thermochemical arguments, the formation of this intermediate can be ruled out, although the formation of the molecular hydrogen−ion complex $(H_2)-M^+-XH_{n-2}$ is not excluded in the exit channel of the molecular hydrogen.

In the following sections, the PESs corresponding to the interaction of iron cation with water, ammonia, and methane, respectively, will be examined. Obviously, for each ligand the reaction paths for both the ground high-spin state and for the excited low one will be properly described. Since the B3LYP/DZVP level of theory yields the wrong ground state for the ion and, therefore, an incorrect reference for the asymptote, the potential energy surfaces calculated at that level are not shown. Contemporary, the results of the topological analysis are reported for the most significant minima and transition states along the paths.

1. Fe^+ Insertion into the O−H Bond. It has been pointed out earlier[29,79,85] that the correct description of the potential energy surface for the insertion reaction of Fe^+ into the O−H bond of water is very challenging due to multiple spin crossing along the reaction path. Moreover, substantial electron correlation effects, both dynamical and nondynamical, complicate further the correct assignment of the spin multiplicity of the species involved. In particular, the spin state of the lowest energy structure of the inserted hydrido iron hydroxyl cation is controversial. Thus, earlier calculations by Schröder et al.[86] suggested that the spin state of the lowest lying structure of the methyl analogue CH_3-Fe^+-OH was a sextet. Afterward, based on higher level calculations on $H-Fe^+-OH$ species, it was claimed that the quartet state should be more stable than the sextet. Although, it should be pointed out that the relative energy between the quartet and sextet states is small, even at the CASPT2D level of theory, namely, 0.55 eV. A recent calculation[29] using CCSD(T) with the TZVP+G(3df,2p) basis set inverted the relative stability, placing the sextet state 0.065 eV lower than the quartet. All of these numbers lie within the error bars of the methods mentioned;[87] hence, they are inconclusive. Interestingly, qualitative arguments could be used to shed light on this stability problem. Thus, Fiedler et al.[85] argue that the quartet state of $H-Fe^+-OH$ benefits from the stability gained by the formation of the H−Fe and O−H covalent bonds, whereas the sextet state should be viewed as a weakly coordination complex between $H^\bullet$ and quintet $FeOH^+$ yielding, therefore, a sextet state for the complex. The energy gained in the sextet relative to the quartet due to the increased number of exchange interaction does not override the energy loss due to the lack of the H−Fe covalent bond. However, an alternative picture emerges from the natural orbital analysis[88] (NBO) of the $^6A'$ state of $H-Fe^+-OH$ carried by Irigoras et al.[29,31] Indeed, their NBO results clearly assign a covalent H−Fe in both the quartet and the sextet states. However, the Fe−O bonding interaction differs markedly between the low- and high-spin states, for the assignment of two paired electrons to the covalent H−Fe bond in the sextet state, and leaves us with a lack of paired electrons for Fe−O bonding. In summary, the emerging picture is that the sextet state is made by unpairing electrons within the nearly degenerate manifold orbitals localized in the Fe−O bonding region, whereas the terminal H−Fe and O−H bonds remain covalent and with two paired electrons each, for both the quartet and sextet states.

TABLE 4: Relative Energies of $FeXH_{n-2}^+ + H_2$ (ΔE), $FeXH_{n-1}^+ + H$ (ΔE_1), and $FeH^+ + XH_{n-1}$ (ΔE_2) Products with Respect to the Ground State of Reactants[a]

system	method	ΔE	ΔE_1	ΔE_2
$Fe^+(^6D) + H_2O$	B3LYP/DZVP[b]	30.0	22.6	51.0
	B3LYP/ $DZVP_{opt}$	37.2	34.2	62.3
	CCSD(T)//B3LYP[b]	37.2	33.1	62.3
	exp.[c]	36.0 ± 1.4	30.4 ± 2.8	$69.2. \pm 1.4$
$Fe^+(^6D) + NH_3$	B3LYP/DZVP	18.7	22.1	37.0
	B3LYP/ $DZVP_{opt}$	31.0	32.7	49.2
$Fe^+(^6D) + CH_4$	B3LYP/DZVP	17.0	34.3	38.7
	B3LYP/ $DZVP_{opt}$	29.9	44.5	47.6
	exp.[d]	29.1 ± 1.2	49.8 ± 1.4	55.6 ± 1.2

[a] The ground states of the products are FeO^+ ($^6\Sigma$), $FeOH^+$ ($^5A'$), FeH^+ ($^5\Delta$), $FeNH^+$ ($^6A'$), $FeNH_2^+$ ($^5A'$), $FeCH_2^+$ ($^4A'$), and $FeCH_3^+$ ($^5A'$). [b] Reference 29. [c] Reference 89. [d] References 41 and 42.

$B3LYP/DZVP_{opt}$ geometrical parameters of stationary points are reported in Figure 1, parts a and b, whereas the corresponding potential energy profile is depicted in Figure 2. In the figures are reported the geometrical parameters for both the B3LYP/DZVP and $B3LYP/DZVP_{opt}$ levels of theory and the relative energies for stationary points obtained at $B3LYP/DZVP_{opt}$ together with CCSD(T)//B3LYP results, reported by Ugalde et al.[29]

In Table 4, the relative energy data for the three main ionic products are compared with previous CCSD(T)//B3LYP[29] results and with the values extracted from the available thermochemical data.[89] The predicted $B3LYP/DZVP_{opt}$ and CCSD(T)//B3LYP ΔE values are in very good agreement with experimental data, whereas energetics given by B3LYP/DZVP computations are, as expected, underestimated.

The first step of the reaction is the exothermic formation of the ion−molecule complex (**I**) along both high and low-spin PESs. BEs for both quartet and sextet states are reported in Table 5 together with values corrected for BSSE. Although the high-spin ground state is the lowest lying at the CCSD(T)//B3LYP level, at the $B3LYP/DZVP_{opt}$ level is the $^4A_1$ the ground state of the complex. In the past,[79] this inverse ordering of the states predicted generally by DF methods in contrast to ab initio methods has been attributed to the already discussed bias in favor of the state with the larger number of 3d electrons. However, this effect cannot be invoked for our B3LYP

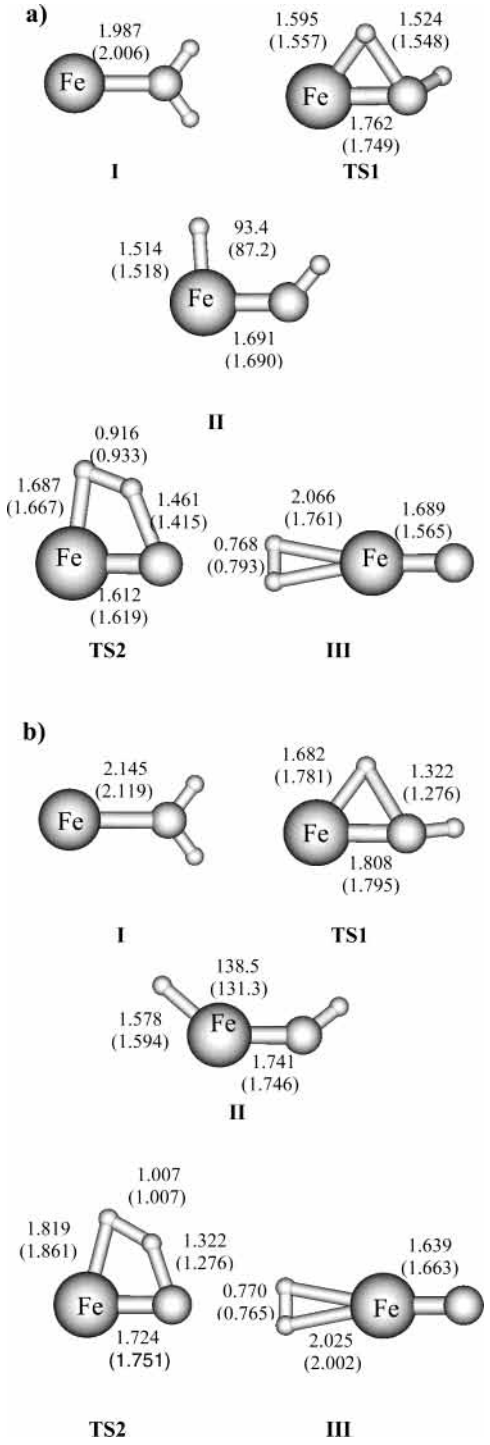

Figure 1. Geometric parameters of minima and transition states on the B3LYP/DZVP$_{opt}$ (a) quartet and (b) sextet potential energy surfaces for the reaction of Fe^+ with H_2O. B3LYP/DZVP parameters are reported in parentheses. Bond lengths are in angstrom and angles in degrees.

calculations performed in conjunction with the new optimized basis set. If we assume the B3LYP/DZVP$_{opt}$ predictions as the correct ones, we meet the first crossing in this region of the PES.

Figure 3 shows the electron localization domains corresponding to all of the important minima and transition states for the lowest-energy spin state species. In that figure, we include the topological structures for the first minima (**I**) corresponding to both, the sextet and quartet electronic spin states. Table 6 reports the topological population analysis for the moieties involved in this reaction. It can be seen that, for the initial complex, the

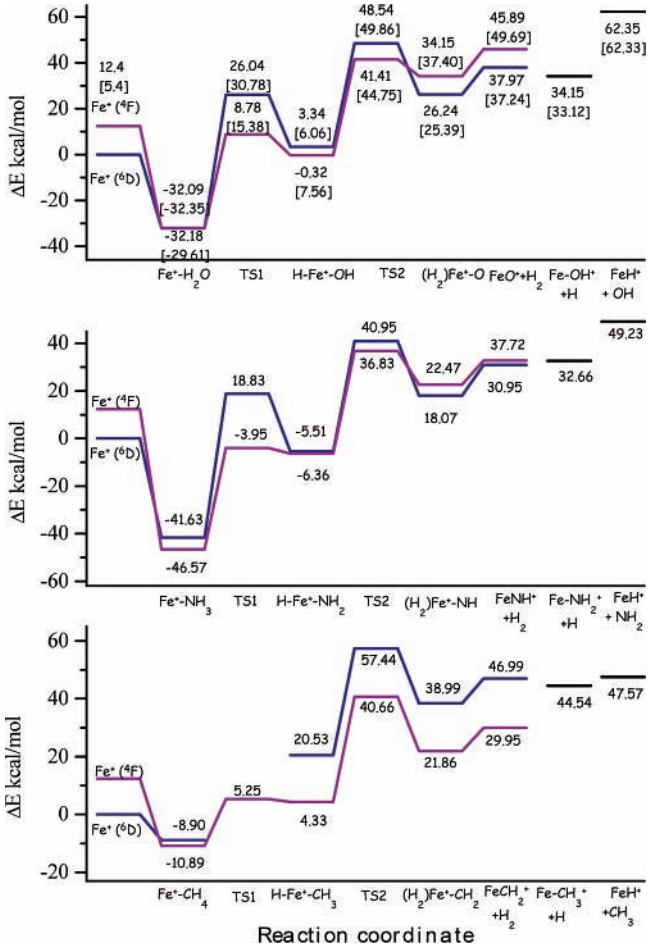

Figure 2. B3LYP/DZVP$_{opt}$ potential energy surfaces for the reactions of Fe^+ with H_2O, NH_3, and CH_4. CCSD(T)//B3LYP relative energies are in square brackets. All the values are in kcal/mol.

TABLE 5: Summary of B3LYP/DZVP$_{opt}$ Binding Energies, Calculated with Respect to the Sextet Ground State of the Cation, for the Quartet (BE_1) and Sextet (BE_2) States of FeH_2O^+, $FeNH_3^+$, and $FeCH_4^+$ Complexes Together with Those Obtained Applying the Counterpoise Correction[a]

complex	BE_1	BE_1(BSSE)	BE_2	BE_2(BSSE)
FeH_2O^+	32.09	31.47	32.18	31.39
$FeNH_3^+$	46.57	45.63	41.63	40.36
$FeCH_4^+$	10.89	11.26	8.90	9.26

[a] All of the values are in kcal/mol.

localization of the V (Fe) basin is quite different depending on the spin multiplicity. In the quartet spin state, V(Fe) presents a particular geometrical distribution that promotes the transfer of charge from this basin toward the ligand. On the contrary, in the case of the sextet spin state the localization of the valence basin does not favor that transfer. The population of the core and valence basins of the $FeOH_2^+$ moieties evidence an interesting behavior that underlines the importance of the different electronic configurations of the quartet and sextet spin states. As seen in Table 6, the core population of Fe^+ in the quartet state is lower than the expectation (i.e., 25 electrons), whereas in the case of the sextet, it is a little higher, since in this case it is expected to find only 24 electrons in the C (Fe) basin (due to its ^6D (sd^6) electronic configuration). Therefore, the V (Fe) basin is populated by 1.22 and 0.87 electrons in the quartet and sextet states, respectively. It is worth noting that in the quartet state the spin density is uniquely located in C (Fe) (see Table 6).

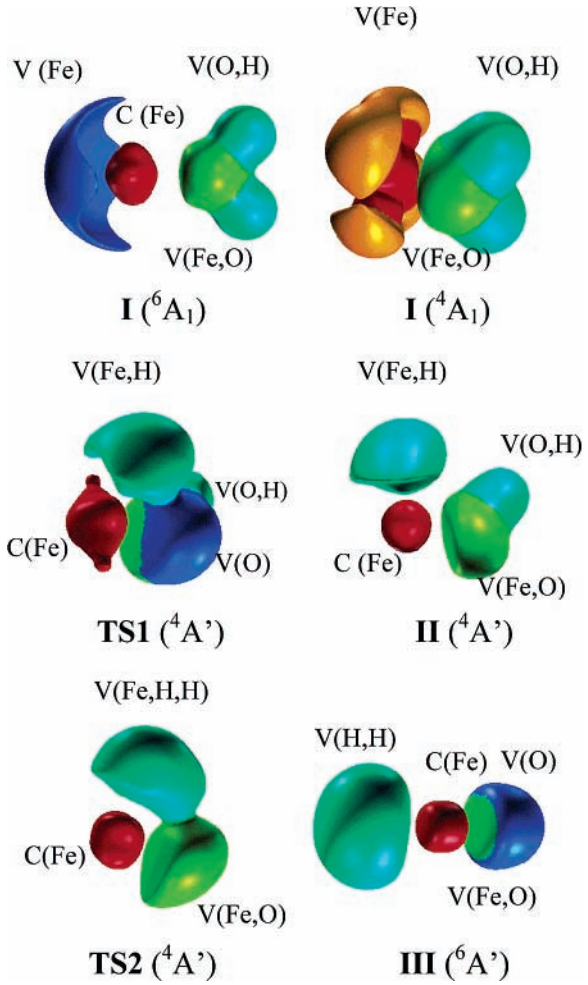

Figure 3. ELF localization domains for all of the key minima involved in the reaction path of the reaction of Fe^+ with H_2O.

The next step of the reaction is the insertion of Fe^+ into the O−H bond of water through the formation of a transition state, **TS1**, which corresponds to the migration of a hydrogen atom from oxygen to the metal. The imaginary frequencies corresponding to the sextet and quartet states are calculated to be 1137*i* and 978*i* cm^{-1}, respectively. The topologies of the two high and low-spin transition states are very similar to each other, but the barriers associated to them are very different, being the activation barrier for quartet significantly lower than sextet. We have justified this fact with the previously discussed favorable geometric localization of the V(Fe) basin in the $^4A_1$ $Fe(H_2O)^+$ complex, which promotes the electron-transfer necessary to the formation of the first transition state. The ELF analysis indicates that an important reorganization of charge takes place when the reaction evolves from the ion−molecule complex to the first transition state. The V(Fe) basin disappears at this point of the reaction, and, at the same time, two other basins appear; i.e., a V(O) monosynaptic basin and the V (H,Fe) disynaptic one (see Figure 3 and Table 6). The C(Fe) population for the **TS1** is very close to 24; therefore, there has been a net electron transfer of nearly one electron toward the ligand, which is now linked to a formal Fe^{2+} cation by a weak dative bond. From **TS1** to the insertion intermediate, the vanishing of the V(O) basin is verified, which promotes a charge transfer to the V(H,Fe) and V(O,Fe) basins. Therefore, the species **I**, **TS1**, and **II** belong to different structural stability domains.[71] The formation of two covalent bonds, H−Fe and Fe−O, as characterized by our ELF analysis, should likely yield a low-spin ground state for the insertion intermediate. The problems in the assignment of the ground state spin multiplicity of this intermediate have yet been widely discussed. Here is pointed out that, at the B3LYP/$DZVP_{opt}$ level, the quartet electromer lies 3.6 kcal/mol lower than its corresponding high-spin sextet state.

From the insertion intermediate (**II**), the reaction proceeds to yield the molecular hydrogen complex $(H_2)FeO^+$ (**III**) after passing through the **TS2** four-center transition state, whose ground-state multiplicity is quartet. The quartet **TS2** structure has an imaginary frequency of 1729*i* cm^{-1}, whereas that for the sextet state is 958*i* cm^{-1}. Looking at the barrier heights, it is worth noting that to obtain the final complex it is necessary to surmount an activation barrier well above the ground-state reactants limit. Since the ion−molecule complex (**III**) corresponds to a sextet multiplicity, between the (**II**) and (**III**) complexes, we find the second cross between high- and low-spin surfaces, in agreement with previous findings. The dehydrogenation products, finally, are formed directly from (**III**) without an energy barrier.

ELF analysis shows that an important rearrangement of charge takes place when the reaction evolves from **II** to **TS2**. This rearrangement involves the formation of a trysinaptic, V(Fe,H,H) basin, at the expense of the vanishing of the V(Fe,H) and the V(O,H) attractors. The resulting basin corresponds to the condensation of two covalent bonds into a three-center bond. The fact that **TS2** involves four nuclear centers, only three of them contributing to the chemical bond, indicates that at this point of the reaction the O−H bond is already essentially broken (d_{O-H} = 1.443 Å at the B3LYP/$DZVP_{opt}$ level). Similar situations are found for the corresponding **TS2**'s for the interactions with ammonia and methane. From a topological point of view, the further evolution of the location of the valence basins is driven mostly by the Pauli repulsion between the V(Fe,H,H) and V(Fe,O) basins.

The dehydrogenation process, as described here, has not been experimentally[90] observed and is not likely to take place under

TABLE 6: Basin Population, $\tilde{N}$, and Integrated Spin Densities, $\langle S_Z \rangle$, of the Key Minima and Transition States Found along the Reaction Path of Fe^+ (^6D,^4F) and H_2O

	I ($^6A_1$)		**I** ($^4A_1$)		**TS1** (^4A)		**II** ($^4A'$)		**TS2** ($^4A'$)		**III** ($^6A'$)		**IV** ($^6\Pi$)	
basin	$\tilde{N}$	$\langle S_Z \rangle$	$\tilde{N}$	$\langle S_Z \rangle$	$\tilde{N}$	$\langle S_Z \rangle$	$\tilde{N}$	$\langle S_Z \rangle$	$\tilde{N}$	$\langle S_Z \rangle$	$\tilde{N}$	$\langle S_Z \rangle$	$\tilde{N}$	$\langle S_Z \rangle$
C(Fe)	24.13	2.06	23.79	1.57	23.96	1.56	23.68	1.45	23.98	1.41	23.85	1.82	23.84	1.85
V(Fe)	0.87	0.37	1.22	−0.09										
C(O)	2.14		2.13		2.12		2.13		2.13		2.11	0.03	2.12	0.03
V(O)					3.16						4.38	0.43	5.58	0.57
V(O,H)	1.70	0.01	1.70		1.80		1.81	0.01						
V(O,Fe)	2.19	0.03	2.17	0.01	2.46		2.89	0.03	3.36	0.04	1.20	0.08	1.45	0.05
V(O,Fe)	2.27	0.03	2.26	0.01			2.72	0.04	3.40	0.05	1.42	0.10		
V(H,Fe)					1.47	−0.08	1.76	−0.04						
V(Fe,H,H)									2.12					
V(H,H)											2.01	0.03		

normal conditions, whereas the observed inverse reaction can proceed through the proposed scheme. The CCSD(T)//B3LYP[29] and B3LYP/DZVP$_{opt}$ descriptions of this region of the PESs are in full agreement, and then, the same conclusions can be drawn with respect to experimental observations. Theoretical results predict an inefficient reaction due to the spin crossover but still having to surmount an energy barrier, in contrast with the experimental evidence of a barrierless reaction as reported by Armentrout et al.[90] In particular, we have found that the quartet **TS2** stays above the FeO^+ ($^6\Sigma$) ground state, and consequently, when the reaction crosses from the sextet PES to the quartet, it must overcome the barrier associated with quartet **TS2**. At higher excitation energies, the system has enough energy to surmount the energy barrier associated with the sextet transition state; therefore, the reaction can proceed along the sextet PES in a spin-conserved way. Previous theoretical results[85] have reported a similar behavior; however, the authors have solved this contradiction indicating an overestimation of about 7 kcal/mol in the quartet states relative to the corresponding sextets, and after this correction, the quartet **TS2** lies nearly degenerate in energy with respect to the sextet $FeO^+ + H_2$ entrance channel.[91]

For the experimentally observed endothermic production of $FeOH^+$ and FeH^+ species, the ground state of the products is compatible with both the high- and low-spin states of the reactants. Thus, formation of $FeOH^+$ and FeH^+ products would not be as sensitive to the reactant state as the dehydrogenation process, and they can be formed by direct bond breaking from both the high- and low-spin electromers of intermediate (**II**).

2. Fe^+ Insertion into the N−H Bond. Detailed experimental observations as well as theoretical investigations of the mechanistic aspects of the interaction of the iron cation with ammonia do not exist in the literature, and this is the first detailed theoretical study of the mechanism of this reaction. Recall, nevertheless, that in 1999 Nakao et al.,[92] reported a detailed study of the reaction of Sc^+, Ni^+, and Cu^+ with ammonia. Potential energy surfaces for high- and low-spin states of the cation, calculated at the B3LYP/DZVP$_{opt}$ level, are sketched in Figure 2. B3LYP/DZVP and B3LYP//DZVP$_{opt}$ geometrical parameters of stationary points are reported in Figure 4, parts a and b.

Our results again suggest that the mechanism of oxidative addition is operative to form the intermediate $H-Fe-NH_2^+$. From this intermediate, the dehydrogenation reaction is predicted to be the most thermodynamically favorable with respect to the other two reaction channels. Table 4 lists the predicted reaction energies. B3LYP/DZVP ΔE values are, as expected, lower than the corresponding B3LYP/DZVP$_{opt}$ ones.

The first step of the reaction of Fe^+ with ammonia is the exothermic formation, along both high- and low-spin PESs, of the ion−molecule complex (**I**), whose ground-state multiplicity is quartet and symmetry C_{3v} (see Figure 4). However, the sextet excited state lies only few kcal/mol above the ground state. In analogy with the water insertion path, a surface crossing is localized yet at the entrance channel of the reaction. The bond dissociation energy of the $FeNH_3^+$ system has been experimentally[44] determined and theoretically calculated,[50] and all of the reported values, compared with those obtained by us, are collected in Table 7, whereas in Table 5, BEs for both quartet and sextet are shown together with the values modified by the introduction of BSSE.

Although the previous theoretical study of Langhoff et al.[50] indicates that the ground state of the adduct is sextet, as exhaustively pointed out by Walter and Armentrout,[44] experimental data appear to be consistent also with the assignment of quartet multiplicity to the $FeNH_3^+$ moiety. Our computed B3LYP/DZVP$_{opt}$ binding energies fit very well the experimental determinations and support a quartet ground state. The B3LYP/

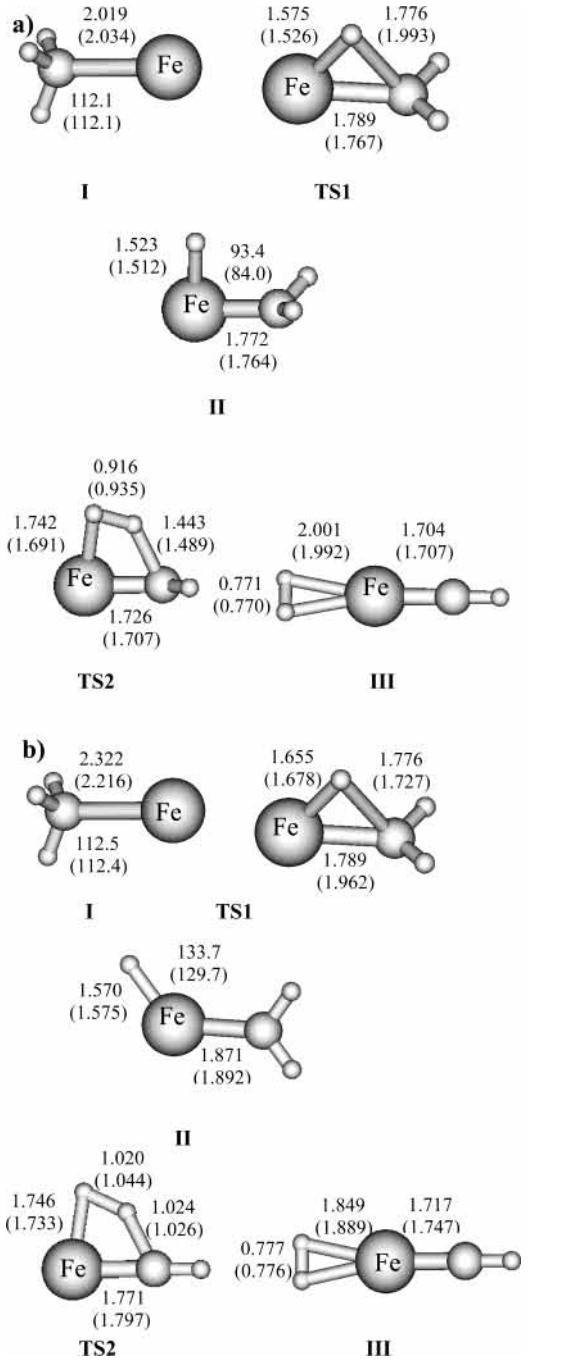

Figure 4. Geometric parameters of minima and transition states on the B3LYP/DZVP$_{opt}$ (a) quartet and (b) sextet potential energy surfaces for the reaction of Fe^+ with NH_3. B3LYP/DZVP parameters are reported in parentheses. Bond lengths are in angstrom and angles in degrees.

TABLE 7: Summary of 0 K Binding Energies (BE), Calculated with Respect to the Sextet Ground State of the Cation, for the Quartet Spin State $FeNH_3^+$ System[a]

level of theory	BE
B3LYP/DZVP	63.9
B3LYP/DZVP$_{opt}$	46.6
MCPF/[8s,6p,4d,1f][b]	45.7
exp.[c]	46.7 ± 2.9

[a] All of the values are in kcal/mol. [b] Reference 50. [c] Reference 44.

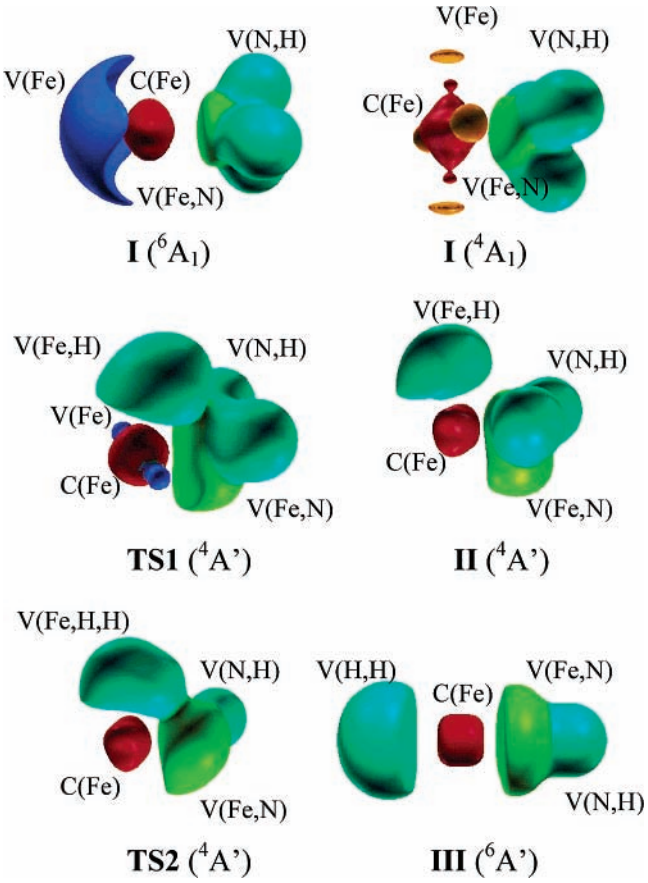

Figure 5. ELF localization domains for all of the key minima involved in the reaction path of the reaction of Fe^+ with NH_3.

DZVP value, reported with the aim of comparison, is obviously out of the mark. The electron localization domains corresponding to key species involved in the reaction of Fe^+ with ammonia are displayed in Figure 5, whereas Table 8 presents the corresponding basin populations and the integrated spin densities. As in the case of the water reaction, the same spin-dependency of the V(Fe) basin's geometrical localization is found for the first ion−molecule complexes. For this reaction, the population of the C(Fe) is of 0.94 electrons for the sextet spin state, whereas the corresponding value for the quartet state is of 1.36 electrons.

The next step of the reaction is the insertion of Fe^+ into the N−H bond of ammonia, to yield the intermediate H−Fe^+−NH_2 (**II**), through the formation of a transition state **TS1**, which corresponds to the shift of a hydrogen atom from nitrogen to the metal. We succeeded in locating the structures, which are three-center complexes, of the transition states related to this process for both the ground low-spin state (ν_i = 630*i* cm^{-1}) and the excited high-spin one (ν_i = 1120*i* cm^{-1}) and is noteworthy that along the quartet surface the barrier height does not exceed the reactants limit. As clearly appears in Figure 4, along the sextet surface, the C_s symmetry of the transition state is not preserved in the product (**II**), which has C_1 symmetry. Since the IRC cannot lose a spatial symmetry while descending from a transition state toward minima along the PES, a *valley-ridge inflection point* (VRI)[93] exists on the C_s-conserved IRC. The **TS1** transition state and the minimum (**II**), therefore, are not directly connected and the terminus of the IRC is another first-order saddle-point which connects two minima that are each other's mirror images with lower symmetry. The possibility of a direct connection of two transition states related to the bifurcation of trajectories has been widely observed[94] and the present system provides a further example of such behavior, which is more common than is generally appreciated.

The ground state of the insertion intermediate seems to have a quartet spin multiplicity even when the difference in energy with respect to the sextet is very small and makes questionable the assignment of the state.

The ELF analysis shows that when the reaction evolves from (**I**) to **TS1** the formation of the V(Fe,H) takes place, which indicates the formation of a weak Fe−H covalent bond. In going from **TS1** to the insertion intermediate (**II**) the increase of the V(Fe,H) basin population, from 1.52 to 1.87 electrons, is made at the expense of the V(Fe) basin, which disappears at this point of the reaction. This fact can be understood as an increase of the 4s orbital contribution to the Fe−H bond. The growth of the V(Fe,H) basin population is an indication of the increase of the Fe−H bond strength. As can be seen in Table 8, the V(Fe) basin is still present in **TS1** and only disappears after surpassing the first transition state, when the system evolves to the formation of the first intermediate (**II**) of the reaction. Consequently, as in the case of the reaction with water, the first transition state, **TS1**, and the intermediate **II** belong to different structural stability domains.

The next step is the formation of the molecular hydrogen complex (H_2)Fe^+−NH (**III**) after overcoming an energy barrier corresponding to a **TS2** four-center transition state, which is high in energy for both high- and low spin-multiplicities. Imaginary frequencies are calculated to be 1671*i* and 1130*i* cm^{-1} for the sextet and quartet states, respectively. On the contrary, the last step of the reaction, the formation of the dehydrogenation products directly from intermediate **III**, occurs without an energy barrier. Due to the height of the barrier which is necessary to overcome to generate the dehydrogenation products (see Figure 2) and since the products are situated well above the energy of the reactants asymptote, only the exothermic formation of the ion−dipole complex and the insertion into the N−H bond are possible at low kinetic energy. A simple breaking of the Fe^+−N and Fe^+−H bonds can generate the other two ionic reaction products directly from the insertion intermediate and is more

TABLE 8: Basin Population, $\tilde{N}$, and Integrated Spin Densities, $\langle S_Z \rangle$, of the Key Minima and Transition States Found along of the Reaction Path of Fe^+ (^{6}D,^{4}F) and NH_3

	I (^{6}A$_1$)		**I** (^{4}A$_1$)		**TS1** (^{4}A′)		**II** (^{4}A′)		**TS2** (^{4}A′)		**III** (^{6}A′)		**IV** (^{6}A$_1$′)	
basin	$\tilde{N}$	$\langle S_Z \rangle$	$\tilde{N}$	$\langle S_Z \rangle$	$\tilde{N}$	$\langle S_Z \rangle$	$\tilde{N}$	$\langle S_Z \rangle$	$\tilde{N}$	$\langle S_Z \rangle$	$\tilde{N}$	$\langle S_Z \rangle$	$\tilde{N}$	$\langle S_Z \rangle$
C(Fe)	24.07	2.02	23.68	1.52	23.42	1.46	23.70	1.48	24.04	1.59	23.90	1.71	23.94	1.75
V(Fe)	0.94	0.40	1.36		0.73	0.06								
C(N)	2.12		2.12		2.12		2.12		2.11	−0.01	2.11	0.03	2.12	0.04
V(N,H)	1.94	0.01	1.95		2.09		2.08	0.01	2.06	−0.03	2.24	0.12	2.38	0.17
V(N,Fe)	2.05	0.06	1.94	0.02	3.01	0.01	3.14	0.01	2.10	−0.01	2.22	0.27	4.54	0.54
V(N,Fe)									2.48	−0.05	2.41	0.29		
V(H,Fe)					1.52	−0.03	1.87							
V(Fe,H,H)									2.20					
V(H,H)											2.11	0.17		

likely to occur than the dehydrogenation process through a tight and complex transition state. From a topological point of view, the formation of **TS2** involves the formation of a trisynaptic V(Fe,H,H) basin, as in the case of the water reaction (see Figure 5).

As underlined by one of the referees of the present work, due to a symmetry change along the path connecting **TS2** and product (**II**), for both multiplicities, a *valley ridge inflection point* would appear also in this case and the steepest descent path starting from **TS2** should stop at a second transition state of higher symmetry, which connects two symmetrically equivalent product minima. We were unable, however, to recognize the existence of VRIs along the paths by using IRC tool, and the difficulties that we met could be ascribed to the lack of symmetry constraints during geometry optimizations of minima and transition states.

3. Fe^+ Insertion into the C−H Bond. Geometrical parameters of stationary points found along the dehydrogenation pathways, for the quartet and sextet states, are reported in Figure 6, parts a and b, whereas their corresponding theoretically predicted PESs are plotted in Figure 2.

The energetics of the three reaction channels leading to the main ionic products of the reaction have been in the past the subject of an interesting debate. In Table 4 are listed the calculated ΔE along with the experimental determinations.[41,42] The theoretical values provided previously by Musaev and Morokuma[45] are 44.5 kcal/mol for the dehydrogenation process and 35 ± 5 kcal/mol for both of the other two channels. Then, the former endothermicity value is underestimated and the latter overestimated with respect the experimental counterparts. On the contrary, our calculated B3LYP/$DZVP_{opt}$ values fit very well the energetics experimentally predicted.

The hypothesised mechanism includes formation, in the entrance channel, of the long-lived ion-induced-dipole complex (**I**), which subsequently yields the insertion intermediate (**II**) by migration of a hydrogen atom corresponding to the transition state **TS1**. The methane complexes (**I**) have the tridentate structures (C_{3v} symmetry), shown in Figure 6, parts a and b, in both, the low and high-spin states, whereas the vibrational analysis of the corresponding bidentate structures confirms their nature of transition states. In Table 9 are collected the binding energies theoretically calculated and experimentally measured for both the high- and low-spin electromers, whereas values corrected for BSSE are reported in Table 5. In disagreement with the previous assignment of a sextet state to the $FeCH_4^+$ adduct,[45] at the employed level of theory, the ground state of the complex is characterized by a quartet spin state with a binding energy that is consistent with the measured value.[92] At the B3LYP/DZVP level, the binding energy of the quartet ground state is abundantly overestimated. CASPT2 computations[96] give also the quartet as the ground state of the complex. If this prediction is assumed to be correct, due to the ground state multiplicity change, in this region of the PES is found the only crossing between the surfaces for this reaction.

The topological characteristics of the ion-methane complex, compared with the corresponding structures for ammonia and water, are modified by the absence of lone pairs in the ligand. This fact justifies the absence of a dysinaptic V(Fe,C) valence basin between the metal and the ligand in the initial complex, in contrast with the reaction of ammonia and water (compare Tables 6, 8, and 10). However, as in the previously described reactions, the topological characteristics of the quartet spin-state V(Fe) basin makes it more suitable to the transfer of charge to the V(Fe,H) basin in comparison with the sextet spin state

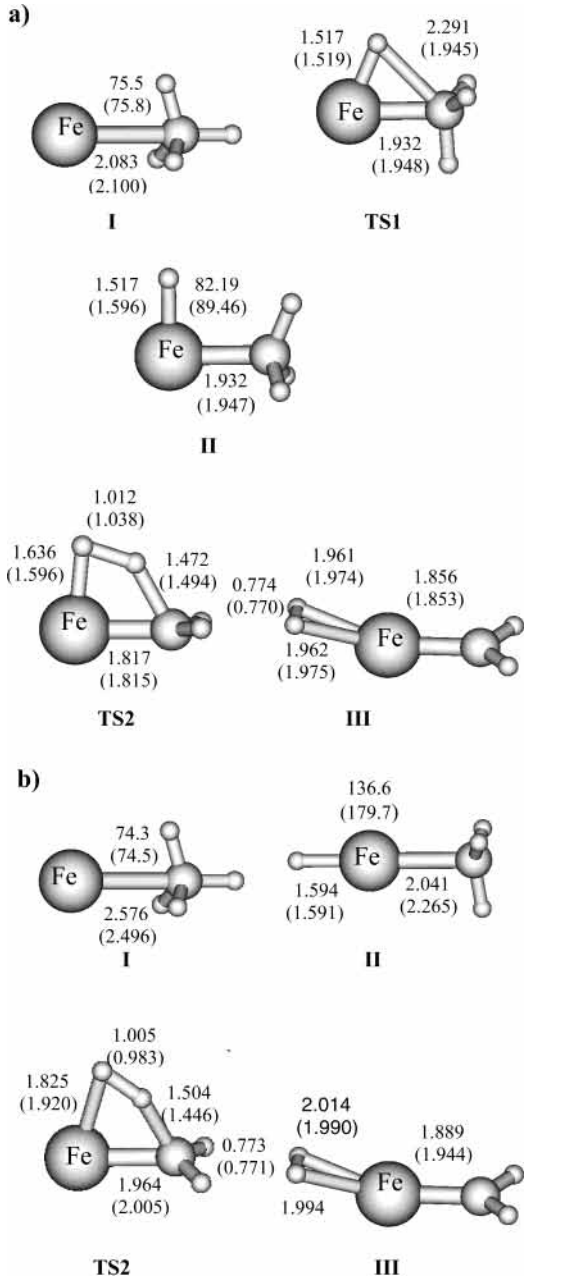

Figure 6. Geometric parameters of minima and transition states on the B3LYP/$DZVP_{opt}$ (a) quartet and (b) sextet potential energy surfaces for the reaction of Fe^+ with CH_4. B3LYP/DZVP parameters are reported in parentheses. Bond lengths are in angstrom and angles in degrees.

TABLE 9: Summary of Binding Energies, Calculated with Respect to the Sextet Ground State of the Cation, for the Quartet (BE_1) and Sextet (BE_2) Spin States of $FeCH_4^+$ Complex[a]

level of theory	BE_1	BE_2
B3LYP/DZVP	32.2	9.9
B3LYP/$DZVP_{opt}$	10.9	8.9
CCSD(T)//B3LYP	15.0	10.9
MR−SDCI−CASSCF(9/9)/BS II+DC[b]	∼2.5	15.5
CASPT2/ANO[c]	13.1	7.7
exp.[d]	13.7 ± 0.8	

[a] All of the values are in kcal/mol. [b] Reference 45. [c] Reference 96. [d] Reference 95.

complex (see Figure 7). The core population of the Fe^+ follows the same trend of the previously described reactions. The localization domains corresponding to key species involved in

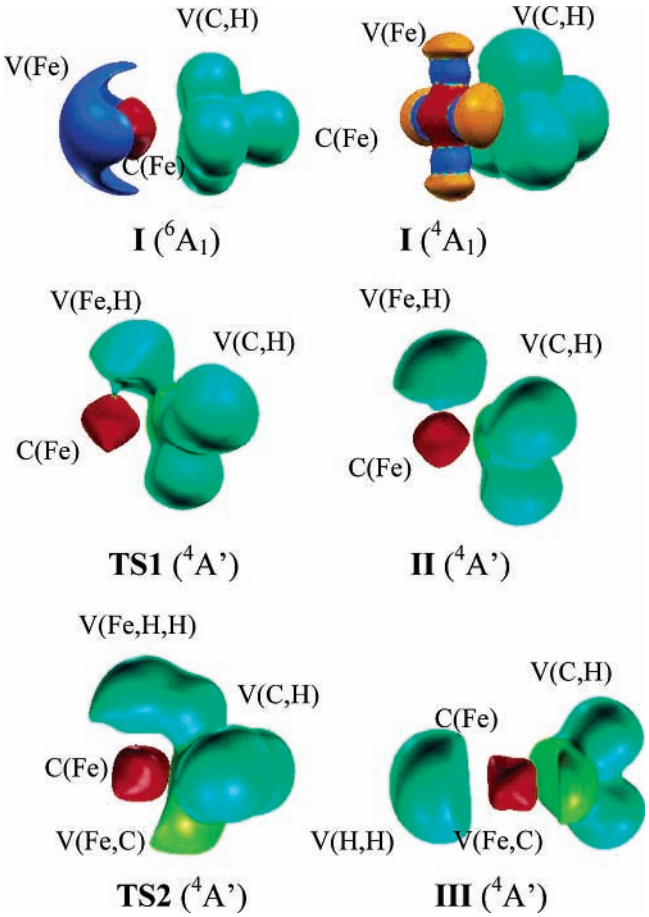

Figure 7. ELF localization domains for all the key minima involved in the reaction path of the reaction of Fe^+ with CH_4.

this reaction are displayed in Figure 7, whereas the quantitative information extracted from the ELF analysis is presented in Table 10.

At the B3LYP/DZVP level any attempt to localize high- and low-spin transition states was unsuccessful, despite the numerous strategies employed. Along the surface investigated using the new $DZVP_{opt}$ basis set together with the B3LYP functional, we succeeded in finding only the quartet ground state ($\nu_i = 630i$ cm^{-1}), which is isoenergetic with the corresponding quartet $H-Fe^+-CH_3$ intermediate. Concerning the insertion intermediate, its existence has also been a matter of discussion. Indeed, experimental data[42] are consistent with the presence along the path of a minimum with the characteristics of the $H-Fe^+-CH_3$ moiety, which bond additivity and more sophisticated estimates indicate to lie about 11 kcal/mol above the sextet asymptote. No stable intermediate is predicted using high-level ab initio calculations. At the CASSCF level, the transition state is lower in energy than the intermediate, which disappears at the CASPT2 level.[46] Also Musaev and Morokuma[45] reached the same conclusion that this minimum does not exist along the PES due to the decreasing of its stability, increasing the level of the theoretical computations. Our results, on the other hand, support the existence of this inserted complex that is a stable minimum situated at 4.3 kcal/mol above the sextet asymptote at the B3LYP/$DZVP_{opt}$ level. ELF analysis indicates that as a consequence of a charge transfer, the V(Fe) basin disappears in going from the first minimum (**I**) to **TS1**. Two valence basins are formed in this step of the reaction, i.e., V(Fe,C) and V(Fe,H) (see Table 10), which indicate the formation of an Fe−C and an Fe−H covalent bond. From this transition state to the intermediate (**II**), there is no topological change in the bonding, which means that the intermediate belongs to the same structural stability domain as **TS1**. Only a small increase of V(H,Fe) population is made at the expense of C(Fe).

The other ion-induced-dipole complex (**III**) found in the exit channel for H_2 elimination is obtained from (**II**) through the four-center transition state, **TS2**. The structures of **TS2** correspond to imaginary frequencies of $1693i$ cm^{-1} for the sextet and of $1324i$ cm^{-1} for the quartet. The energy barrier associated with the quartet ground state of this species is very high, and then, our findings are in perfect agreement with the previous conclusion that the dehydrogenation of methane by Fe^+ is hindered by a tight four-center transition state. The height of the barrier relative to the formation of the same transition state, but for the reverse reaction ($FeCH_2^+ + H_2$), can be compared with the conflicting experimentally (9.8 ± 1.4 kcal/mol) and theoretically (22.0 kcal/mol) determined values. The values of about 19 kcal/mol is consistent with the theoretical value.

After overcoming the **TS2** transition state, the molecular hydrogen complex (**III**) is formed, and due to the quartet multiplicity in the ground state, the spin is conserved in the last step of the reaction. From that species, the loss of an H_2 molecule occurs without an energy barrier and gives one of the experimentally not observed reaction products. As in the case of the two previous reactions, the formation of **TS2** is characterized by the condensation of two disynaptic basins, V(Fe,H) and V(C,H) generate a trisynaptic V(Fe,H,H) basin, indicating the presence of a three-center bond (see Table 10 and Figure 7). Reactions to generate $FeCH_3^+$ and FeH^+ fragments are simply uphill from the hydridomethyl intermediate $H-Fe^+-CH_3$ and take place through simple metal−hydrogen and metal−carbon bond cleavages. These two exit channels are situated at about 45 and 50 kcal/mol above the entrance channel and are more endothermic than the dehydrogenation one. At moderate temperatures, then, only one stable product can be obtained, the ion−molecule complex, $FeCH_4^+$, and at least the inserted complex can be accessible. Although the endothermicity of the

TABLE 10: Basin Population, $\tilde{N}$, and Integrated Spin Densities, $\langle S_Z \rangle$, of the Key Minima and Transition States Found along of the Reaction Path of Fe^+ (^{6}D,^{4}F) and CH_4

	I ($^6A_1$)		**I** ($^4A_1$)		**TS1** ($^4A'$)		**II** ($^4A'$)		**TS2** ($^4A'$)		**III** ($^4A'$)		**IV** ($^4B_1$)	
basin	$\tilde{N}$	$\langle S_Z \rangle$	$\tilde{N}$	$\langle S_Z \rangle$	$\tilde{N}$	$\langle S_Z \rangle$	$\tilde{N}$	$\langle S_Z \rangle$	$\tilde{N}$	$\langle S_Z \rangle$	$\tilde{N}$	$\langle S_Z \rangle$	$\tilde{N}$	$\langle S_Z \rangle$
C(Fe)	24.28	2.12	23.61	1.46	24.00	1.46	23.80	1.51	23.86	1.47	24.00	1.66	24.14	1.73
V(Fe)	0.75	0.32	1.35	0.01									0.12	0.03
C(C)	2.11		2.11		2.11		2.11		2.10		2.10	−0.02	2.10	−0.02
V(C,H)	1.99	0.02	1.98	0.01	2.05		2.05		2.06		2.05	−0.06	2.09	−0.07
V(C,Fe)					1.00		1.03		2.22	0.08	1.15		1.22	−0.05
V(C,Fe)											1.52	−0.02	1.23	−0.05
V(H,Fe)					1.75	0.02	1.82							
V(Fe,H,H)									2.68	−0.03				
V(H,H)											2.10	0.01		

reactions that give the $FeCH_3^+$ and FeH^+ products are less favorable, the requirement of a large activation energy makes hydrogen elimination from methane less probable, at elevated temperatures, with respect to the other two channels. Moreover, if the quartet excited ground state is assumed as the dissociation limit, all of the considered reactions are less endothermic by few kcal/mol and no unfavorable intersystem crossing is required, and in agreement with experimental observations, the quartet state is expected to be much more reactive than the sextet one.

IV. Comparison between PESs

In this section, we summarize and compare the behaviors along the paths for the insertion of the iron cation into the O−H, N−H, and C−H bonds of water, ammonia, and methane, trying to explain their similarities and differences. First of all, the stabilization energy of the ion−dipole complex (**I**) with respect to the reactants decreases in going from ammonia to water to methane. As previously pointed out,[50] the bond formed between the ion and the non inserted ligand is not simply electrostatic in nature and its strength is determined by a balance between the electrostatic interaction, charge donation from the ligand to the metal cation, and the Pauli repulsion. Recall that the low-spin ^4F (d^7) excited state of Fe^+ can easily accommodate electron density from the donor ligand in its vacant 4s orbital. Still, the three unpaired electrons in its d shell remain to render the correct quartet spin state. Hence, good electron donors such as ammonia will tend to stabilize this low-spin state. Conversely, the dominant configuration of the high-spin ^6D (sd^6) ground state of Fe^+ is $4s^1 3d_{-1}^1 3d_0^1 3d_1^1$ $1/\sqrt{2}(3d_2^1 3d_{-2}^2 \pm 3d_2^2 3d_{-2}^1)$. Accepting electron density from the donor triggers a strong Pauli repulsion for some of the unpaired electrons, required to yield the sextet spin multiplicity. Therefore, bonding between the ligand and the iron cation's sextet ground state will be largely electrostatic. Water having a markedly large partial charge on oxygen and sizeable dipole moment should stabilize this high-spin state. Our calculations confirm this qualitative reasoning. Finally, methane is found to stabilize the quartet state by 2 kcal/mol with respect to the sextet. This suggests that the donation from the three η^3-donor hydrogens of CH_4 to the vacant 4s orbital of ^4F state of Fe^+ dominates over the polarization interaction between the sextet ^6D ground state of Fe^+ and the unpolar methane molecule.

The next minimum along the surfaces is the low-spin H−Fe-XH_{n-1} complex (**II**), whose ground-state multiplicity is quartet in all cases except for the H−Fe^+−OH intermediate at the CCSD(T)//B3LYP level of theory. From Figure 2, it is clear that none of them are significantly lower in energy than the dissociation limit and the presence of lone pairs does not enhance the stability as it happens for other ions of the same series. This is a general feature that can be drawn on the basis of our results and that can be extended also to the other stationary points along the energy profiles.

The transition states, **TS1**, all of low-spin multiplicity in the ground state have very similar structures, but in going from water to ammonia and methane, the bond distance between the X atom and the transferring hydrogen progressively elongates until the bond is completely broken. In parallel, the barrier height lowers and the energy difference with respect to the insertion products becomes very small for ammonia and methane. However, only when the hydrogen shift involves the N atom, the barrier height is found below the $Fe^+(^6D)+NH_3$ asymptote.

After the formation of the insertion intermediate, the most relevant remark is the presence of a second surface crossing along the PESs for water and ammonia to obtain products whose ground-state spin multiplicity is the same as that for the reactants. The most stable final ion−dipole complexes (**III**) have, obviously, the same multiplicity of dehydrogenation products being the molecular hydrogen practically formed. Geometrical parameters of products in their ground states are reported in Table 11. The existence of a double bond between iron and X atoms corresponds to very similar binding energies and endothermicities with respect to reactants. Then, the energy barriers that are necessary to overcome to generate the final ion−dipole complex (**III**) correspond to the activation energies along the paths for the three ligands. The barrier heights are in all cases well above the ground-state asymptotes and are comparable among them.

TABLE 11: Equilibrium Geometry Parameters for Ground-State $FeXH_{n-2}^+$ Dehydrogenation Products at the B3LYP/DZVP, in Parentheses, and B3LYP/$DZVP_{opt}$ Levels of Theory[a]

product	M−X	X−H	M−X−H
FeO^+	(1.636[b])		
	1.772		
$FeNH^+$	(1.712)	(1.020)	
	1.729	1.020	
$FeCH_2^+$	(1.841)	(1.099)	(123.1)
	1.895	1.089	118.8

[a] Bond lengths are in Å and angles in degrees. [b] Reference 29.

The topological analysis of the ELF function indicates that for the first stage of the reaction, i.e., till the formation of the first intermediate, the main difference found between the three studied reactions are a consequence of the presence/absence of lone-pairs in the ligand. The presence of lone pairs in NH_3 and H_2O determines the formation of a disynaptic basin, V(Fe,X) (for X = N,O), in the first ion−molecule complexes (see Tables 6 and 8). The main electronic contribution to these basins comes, in almost 90%, from the contribution of the ligand lone pairs. For the methane reaction, the corresponding basin is present only after the formation of the first transition state. For the three reactions, the evolution to the first transition state involves the formation of a disynaptic V(Fe,H) basin, and, in the case of CH_4 the formation of another disynaptic, V(Fe,C) basin, which, as was just mentioned was absent in the ion−molecule complex. These new basins are formed at expenses of the V(Fe) basin population, which disappear (in the case of the reaction of CH_4 and H_2O) at this point of the reaction. It is worth noting that, in the case of ammonia, this monosynaptic V(Fe) basin is still present in the **TS1** (see Table 8), whereas in the case of water, a monosynaptic V(O) basin is found instead.

In the case of the methane reaction, there is no topological changes in going from **TS1** to **II**, i.e., both structures belong to the same structural stability domain. A small increase in the V(Fe,H) basin population indicates the growth of the Fe−H covalent bond strength. In the case of the ammonia reaction, instead, the passage to **II** involves the charge transfer of the V(Fe) basin population to the V(N,Fe) and V(Fe,H) dysinaptic basins, which increases in this way its populations. Similar rearrangements of charge are verified in going from **TS1** to **II** for the reaction with water, but, in this case the electronic charge comes from the vanishing of the V(O) basin. Therefore, the main differences in the charge reorganizations that take place during the first part of the reaction are a consequence of the different number of lone pairs present in the ligands.

After the formation of the first insertion intermediate (**II**) the reactions are quite similar from a topological point of view. The transition from intermediate (**II**) to **TS2** is achieved through

the increase of the V(Fe,X) population, which gains 1.19, 1.44, and 1.15 electrons for CH_4, NH_3, and H_2O, respectively. These gains are mostly due to a charge transfer from the V(Fe,H) and V(X,H) basins, which reunify into a single V(Fe,H,H) basin. The main topological characteristic of the second transition state is the presence of this trysinaptic basin. The formation of the last intermediate state (**III**) involves rather small charge transfers in the case of the reaction of CH_4 and NH_3. In the case of the reaction of methane, on one hand, the V(Fe,H,H) population tends to two in order to enable the further detachment of the H_2 molecule. On the other hand, this charge loss induces a transfer toward the C(Fe) and V(C,Fe) basins for the reaction with methane (Table 10). In the case of ammonia, the V(Fe,N) population is already very high at **TS2**, and therefore, the electronic reorganization tends to spread the electron density. The further evolution of the valence basins is driven mostly by the Pauli repulsion between the V(Fe,H,H) and V(Fe,X) basins. The behavior of water in its lowest-energy sextet spin complex is rather different since, as the result of the detachment of the H_2 molecule, an important redistribution of charge takes place, and the V(O) is formed.

V. Conclusions

The reactions of the iron cation with water, ammonia, and methane have been computed and analyzed. Both high- and low-spin potential energy surfaces have been characterized in detail at the B3LYP level and using a newly developed DZVP basis set optimized ad hoc for the employed functional. The results obtained at the B3LYP level in conjunction with the traditional DZVP basis set optimized in the framework of the local approximation give the wrong ground state for the ion, and then the potential energy surfaces calculated at that level are not shown, also if some energetical data are commented. The energy diagrams are in all cases uphill toward formation of dehydrogenation products, and at low kinetic energies, only the exothermic formation of the first ion−dipole complex is possible. Moreover, at high temperatures, also when the endothermicity of the reactions that give the $FeXH_{n-1}^+$ and FeH^+ products are less favorable, the necessity to overcome a high energy barrier makes hydrogen elimination from the ligand less probable than the other two reaction channels. Our calculations confirm that high- and low-spin potential energy surfaces have crossing points, in correspondence of which spin inversion takes place. Two surface crossings are present along the paths for the insertion into O−H and N−H bonds, and consequently, the spin is conserved, whereas the single crossing at the entrance channel of the insertion reaction into the C−H bond can be avoided if the quartet excited state is assumed as the dissociation limit. The picture of the behaviors along the paths has been supported by a topological description, based on the gradient field analysis of the electron localization function, of all of the key minima and transition states along the reaction pathways in order to characterise the bonding.

Acknowledgment. This research was funded by Euskal Herriko Unibertsitatea (the University of the Basque Country), Eusko Jaurlaritza (the Basque Government), the Spanish Science and Technology Office, and by Università degli Studi della Calabria and MIUR.

References and Notes

(1) Freas, R. B.; Ridge, D. P. *J. Am. Chem. Soc.* **1980**, *102*, 7129.
(2) Aristov, A.; Armentrout, P. B. *J. Am. Chem. Soc.* **1984**, *106*, 4065.
(3) Tolbert, M. A.; Beauchamp, J. L. B. *J. Am. Chem. Soc.* **1984**, *106*, 8117.
(4) Reents, W. L.; Strobel, F.; Freas, R. B.; Wronka, J.; Ridge, D. P. *J. Phys. Chem.* **1985**, *89*, 5666.
(5) Aristov, N.; Armentrout, P. B. *J. Phys. Chem.* **1986**, *108*, 1806.
(6) Kang, N.; Beauchamp, J. L. *J. Am. Chem. Soc.* **1986**, *108*, 7502.
(7) Aristov, N.; Armentrout, P. B. *J. Phys. Chem.* **1987**, *91*, 6178.
(8) Sunderlin, L. S.; Armentrout, P. B. *J. Phys. Chem.* **1988**, *92*, 1209.
(9) Georgiadis, R.; Armentrout, P. B. *J. Phys. Chem.* **1988**, *92*, 7067.
(10) Buckner, S. W.; Gord, J. R.; Freiser, B. S. *J. Am. Chem. Soc.* **1988**, *110*, 6606.
(11) Irikura, K. K.; Beauchamp, J. L. *J. Am. Chem. Soc.* **1989**, *111*, 75.
(12) Sunderlin, L. S.; Armentrout, P. B. *J. Am. Chem. Soc.* **1989**, *111*, 3845.
(13) Magnera, T. F.; David, D. E.; Michl, J. *J. Am. Chem. Soc.* **1989**, *111*, 4100.
(14) Armentrout, P. B.; Beauchamp, J. L. *Acc. Chem. Res.* **1989**, *22*, 315.
(15) Russel, D. H., Ed. *Gas-Phase Inorganic Chemistry*; Plenum: New York, 1989; p 412.
(16) Armentrout, P. B. *Annu. Rev. Phys. Chem.* **1990**, *41*, 313.
(17) Clemmer, D. E.; Sunderlin, L. S.; Armentrout, P. B. *J. Phys. Chem.* **1990**, *94*, 208.
(18) Clemmer, D. E.; Sunderlin, L. S.; Armentrout, P. B. *J. Phys. Chem.* **1990**, *94*, 3008.
(19) Armentrout, P. B. *Science* **1991**, *41*, 175.
(20) Fisher, E. R.; Armentrout, P. B. *J. Am. Chem. Soc.* **1992**, *114*, 2049.
(21) Guo, B. C.; Kerns, K. P.; Castleman, A. W. *J. Phys. Chem.* **1992**, *96*, 4879.
(22) Clemmer, D. E.; Aristov, N.; Armentrout, P. B. *J. Phys. Chem.* **1993**, *97*, 544.
(23) Chen, Y.; Clemmer, D. E.; Armentrout, P. B. *J. Phys. Chem.* **1994**, *98*, 11490.
(24) Chen, Y.; Armentrout, P. B. *J. Phys. Chem.* **1995**, *99*, 10775.
(25) Haynes, C. L.; Chen, Y.; Armentrout, P. B. *J. Phys. Chem.* **1995**, *99*, 9110.
(26) Freiser, B. S. *J. Mass Spectrom.* **1996**, *31*, 703.
(27) Irigoras, A.; Fowler, J. E.; Ugalde, J. M. *J. Phys. Chem.* **1998**, *102*, 293.
(28) Irigoras, A.; Fowler, J. E.; Ugalde, J. M. *J. Am. Chem. Soc.* **1999**, *121*, 574.
(29) Irigoras, A.; Fowler, J. E.; Ugalde, J. M. *J. Am. Chem. Soc.* **1999**, *121*, 8549.
(30) Irigoras, A.; Elizalde, O.; Silanes, I.; Fowler, J. E.; Ugalde, J. M. *J. Am. Chem. Soc.* **2000**, *122*, 114.
(31) Irigoras, A. *Water Dehydrogenation by First-Row Transition Metal Cations. A Paradigm for Two-State Reactivity*; Euskal Herriko Unibertsitatea Press: Bilbao, Euskadi, Spain, 1999.
(32) Abashkin, Y. G.; Burt, S. K.; Russo, N. *J. Phys. Chem.* **1997**, *101*, 8085.
(33) Russo, N.; Sicilia, E. *J. Am. Chem. Soc.* **2001**, *123*, 2588.
(34) Russo, N.; Sicilia, E. *J. Am. Chem. Soc.* **2002**, *124*, 1471.
(35) Michelini, M. C.; Russo, N.; Sicilia, E. *J. Phys. Chem.* **2002**, *106*, 8937.
(36) Schroder, D.; Shaik, S.; Schwarz, H. *Acc. Chem. Res.* **2000**, *33*, 139.
(37) Armentrout, P. B.; Beauchamp, J. L. *Acc. Chem. Res.* **1989**, *22*, 315.
(38) Armentrout, P. B. *Science* **1991**, *251*, 175.
(39) Bruckner, S. W.; Gord, J. R.; Freiser, B. S. *J. Am. Chem. Soc.* **1988**, *110*, 6606.
(40) Tonkyn, R.; Ronan, M.; Weisshaar, J. C. *J. Phys. Chem.* **1988**, *92*, 92.
(41) Schultz, R. H.; Elkind, J. L.; Armentrout, P. B. *J. Am. Chem. Soc.* **1988**, *110*, 411.
(42) Haynes, C. L.; Chen, Y.; Armentrout, P. B. *J. Phys. Chem.* **1996**, *100*, 111.
(43) Jacobson, D. B.; Freiser, B. S. *J. Am. Chem. Soc.* **1985**, *107*, 5870.
(44) Walter, D.; Armentrout, P. B. *J. Am. Chem. Soc.* **1998**, *120*, 3176.
(45) Musaev, D. G.; Morokuma, K. *J. Chem. Phys.* **1994**, *101*, 10697.
(46) Hendrickx, M.; Ceulemans, M.; Gong, K.; Vanquickenborne, L. *J. Phys. Chem.* **1997**, *101*, 2465.
(47) Ricca, A.; Bauschlicher, C. W., Jr.; Rosi, M. *J. Phys. Chem.* **1994**, *98*, 9498.
(48) Ricca, A.; Bauschlicher, C. W., Jr. *Theor. Chim. Acta* **1995**, *92*, 123.
(49) Tsipis, A. C. *J. Chem. Soc., Faraday Trans.* **1998**, *94*, 11.
(50) Langhoff, S. R.; Bauschlicher, C. W., Jr.; Partridge, H.; Sodupe, M. *J. Phys. Chem.* **1991**, *95*, 10677.
(51) See, for example: (a) Gunnarson, O.; Jones, R. O. *Phys. Rev. B.* **1985**, *31*, 7588. (b) Ziegler, T.; Li, J. *Can. J. Chem.* **1994**, *72*, 783.
(52) Becke, A. D. *J. Chem. Phys.* **1993**, *98*, 5648.
(53) Lee, C.; Yang, W.; Parr, R. G. *Phys. Rev. B* **1988**, *37*, 785.
(54) (a) Andzelm, J.; Radzio, E.; Salahub, D. R. *J. Comput. Chem.* **1985**, *6*, 520. (b) Goudbout, N.; Salahub, D. R.; Andzelm, J.; Wimmer, E. *Can. J. Chem.* **1992**, *70*, 560.
(55) Fukui, K. *J. Chem. Phys.* **1970**, *74*, 4161.
(56) Aschi, M.; Brönstrup, M.; Diefenbach, M.; Harvey, J. N.; Schröder, D.; Schwarz, H. *Angew. Chem., Int. Ed. Engl.* **1998**, *37*, 829.

(57) Ricca, A.; Bauschlicher, C. W., Jr. *Chem. Phys. Lett*. **1995**, *245*, 150.
(58) Holthausen, M. C.; Fiedler, A.; Schwarz, H.; Koch, W. *J. Phys. Chem*. **1996**, *100*, 6236.
(59) Bauschlicher, C. W. Jr.; Ricca, A.; Partridge, H.; Langghoff, S. R. In *Recent Advances in Density Functional Theory*; Chong, D. P., Ed.; World Scientific Publishing Co.: Singapore, 1997; Part II and references therein.
(60) Sodupe, M.; Branchadell, V.; Rosi, M.; Bauschlicher, C. W., Jr. *J. Phys. Chem*. **1997**, *101*, 7854.
(61) Pavlov, M.; Siegbahn, P. E. M.; Sandström, M. *J. Phys. Chem. A* **1998**, *102*, 219.
(62) Yi, S. S.; Blomberg, M. R. A.; Siegbahn, P. E. M.; Weisshaar, M. *J. Phys. Chem*. **1998**, *102*, 395.
(63) Holthausen, M. C.; Koch, W. *J. Am. Chem. Soc*. **1996**, *118*, 9932.
(64) Gianolio, L.; Pavani, R.; Clementi, E. *Gazzetta Chim. Ital*. **1978**, *108*, 181.
(65) Boys, S. B.; Bernardi, F. *Mol. Phys*. **1970**, *19*, 553.
(66) Frisch, M. J.; Trucks, G. W.; Schlegel, H. B.; Gill, P. M. W.; Johnson, B. G.; Robb, M. A.; Cheeseman, J. R.; Keith, T. A.; Petersson, G. A.; Montgomery, J. A.; Raghavachari, K.; Al-Laham, M. A.; Zakrzewski, V. G.; Ortiz, J. V.; Foresman, J. B.; Croslowski, J.; Stefanov, B. B.; Nanayakkara, A.; Challacombe, M.; Peng, C. Y.; Ayala, P. Y.; Chen, W.; Wong, M. W.; Andres, J. L:, Replogle, E. S.; Gomperts, R.; Martin, R. L.; Fox, D. J.; Binkley, J. S.; Defrees, D. J.; Baker, J.; Stewart, J. P.; Head-Gordon, M.; Gonzales, C.; Pople, J. A. *Gaussian 94*, revision A.1; Gaussian, Inc.: Pittsburgh, PA, 1995.
(67) Silvi, B.; Savin, A. *Nature* **1994**, *371*, 683.
(68) Becke, A. D.; Edgecombe, K. E. *J. Chem. Phys*. **1990**, *92*, 5397.
(69) Savin, A.; Nesper, R.; Wengert, S.; Fässler, T. F. *Angew. Chem., Int. Ed. Engl*. **1997**, *36*, 1809.
(70) Noury, S.; Silvi, B.; Gillespie, R. G.; *Inorg. Chem*. **2002**, *41*, 2164.
(71) Krokidis, X.; Noury, S.; Silvi, B. *J. Phys. Chem. A* **1997**, *101*, 7277.
(72) Krokidis, X.; Vuilleumier, R.; Borgis, D.; Silvi, B. *Mol. Phys*. **1999**, *96*, 265.
(73) Krokidis, X.; Moriarty, N. W.; Lester, W. A., Jr.; Frenklach, M. *Chem. Phys. Lett*. **1999**, *314*, 534.
(74) Michelini, M. C.; Sicilia, E.; Russo, N.; Alikhani, E.; Silvi, B. *J. Phys. Chem. A* **2003**, *107*, 4862.
(75) Noury, S.; Krokidis, X.; Fuster, F.; Silvi, B. *TopMod Package*; Paris, 1997.
(76) Noury, S.; Krokidis, X.; Fuster, F.; Silvi, B. *Comput. Chem*. **1999**, *23*, 597.
(77) Pepke, E.; Muray, J.; Lyons, J. *Scian (Supercomputer Computations Res. Inst.)*; Florida State University: Tallahassee, FL, 1993.
(78) Moore, C. E. *Atomic Energy Levels*; NSRD-NBS, U.S.A.; U.S. Government Printing Office: Washington, DC, 1991; Vol. 1.
(79) Ricca, A.; Bauschlicher, C. W., Jr. *J. Phys. Chem*. **1995**, *99*, 9003.
(80) Filatov, S.; Shaik, S. *J. Phys. Chem. A* **1998**, *102*, 3835.
(81) Loh, S. K.; Fisher, L.; Lian, E. R.; Schultz, R. H.; Armentrout, P. B. *J. Phys. Chem*. **1989**, *93*, 3159.
(82) Schultz, R. H.; Armentrout, P. B. *Organometallics* **1992**, *11*, 828.
(83) Fisher, E. R.; Schultz, R. H.; Armentrout, P. B. *J. Phys. Chem*. **1989**, *93*, 7382.
(84) Elkind, J. L.; Armentrout, P. B. *J. Am. Chem. Soc*. **1986**, *108*, 2765; *J. Phys. Chem*. **1986**, *90*, 5736.
(85) Fiedler, A.; Schröder, D.; Shaik, S.; Schwarz, H. *J. Am. Chem. Soc*. **1994**, *116*, 10734.
(86) Schröder, D.; Fiedler, A.; Hrušák, J.; Schwarz, H. *J. Am. Chem. Soc*. **1992**, *114*, 1215.
(87) Klopper, W.; Bak, K. L.; Jørgensen, P.; Olsen, J.; Helgaker; T. J. *Phys. B*. **1999**, *32*, R103.
(88) Read, A. E.; Curtiss, L. A.; Weinhold, F. *Chem. Rev*. **1988**, *88*, 899.
(89) Chase, M. W.; Davies, C. A.; Downey, J. R.; Frurip, D. J.; McDonald, R. A.; Syvened, A. N. *J. Phys. Chem. Ref. Data*, *14*, Suppl. N 1 (JANAF Tables), 1985.
(90) Clemmer, D. E.; Chen, Y.; Khan, F. A.; Armentrout, P. B. *J. Phys. Chem*. **1994**, *98*, 6522.
(91) Danovich, D.; Shaik, S. *J. Am. Chem. Soc*. **1997**, *119*, 1773.
(92) Nakao, Y.; Taketsugu, T.; Hirao, K. *J. Chem. Phys*. **1999**, *110*, 10863.
(93) Valtazanos, P.; Elbert, S. T; Xantheas, S.; Ruedenberg, K. *Theor. Chim. Acta* **1991**, *78*, 287. Xantheas, S.; Valtazanos, P.; Ruedenberg, K. *Theor. Chim. Acta* **1991**, *78*, 327. Xantheas, S.; Valtazanos, P.; Ruedenberg, K. *Theor. Chim. Acta* **1991**, *78*, 327. Xantheas, S.; Elbert, S. T.; Ruedenberg, K. *Theor. Chim. Acta* **1991**, *78*, 365. Valtazanos, P.; Ruedenberg, K. *Theor. Chim. Acta* **1991**, *78*, 397.
(94) See, for example: Kumeda, Y.; Taketsugu, T. *J. Chem. Phys*. **2000**, *113*, 477. Taketsugu, T.; Tajima, N.; Hirao, K. *J. Chem. Phys*. **1996**, *105*, 1933. Yanai, T.; Taketsugu, T.; Hirao, K. *J. Chem. Phys*. **1997**, *107*, 1137. Bartsch, R. A.; Chae, Y. M. C.; Ham, S.; Birney, D. M. *J. Am. Chem. Soc*. **2001**, *123*, 7479. Quapp, W.; Melnikov, V. *Phys. Chem. Chem. Phys*. **2001**, *3*, 2735. Singleton, D. A.; Hang, C.; Szymanski, M. J.; Meyer, M. P.; Leach, A. G.; Kuwata, K. T.; Chen, J. S.; Greer, A.; Foote, C. S.; Houk, K. N. *J. Am. Chem. Soc*. **2003**, *125*, 1319.
(95) Schultz, R. H.; Armentrout, P. B. *J. Phys. Chem*. **1993**, *97*, 596.
(96) Hendrickx, M.; Gong, K.; Vanquickenborne, L. *J. Chem. Phys*. **1997**, *107*, 6299.